MOLECULAR AND CELLULAR BIOLOGY, June 2005, p. 4625–4637 Vol. 25, No. 11
0270-7306/05/$08.00+0 doi:10.1128/MCB.25.11.4625–4637.2005

YB-1 Is Important for Late-Stage Embryonic Development, Optimal Cellular Stress Responses, and the Prevention of Premature Senescence

Zhi Hong Lu, Jason T. Books, and Timothy J. Ley*

Division of Oncology, Departments of Medicine and of Genetics, Siteman Cancer Center, Washington University School of Medicine, St. Louis, Missouri 63110

Received 17 December 2004/Returned for modification 5 February 2005/Accepted 25 February 2005

Proteins containing "cold shock" domains belong to the most evolutionarily conserved family of nucleic acid-binding proteins known among bacteria, plants, and animals. One of these proteins, YB-1, is widely expressed throughout development and has been implicated as a cell survival factor that regulates the transcription and/or translation of many cellular growth and death-related genes. For these reasons, YB-1 deficiency has been predicted to be incompatible with cell survival. However, the majority of *YB-1*$^{-/-}$ embryos develop normally up to embryonic day 13.5 (E13.5). After E13.5, *YB-1*$^{-/-}$ embryos exhibit severe growth retardation and progressive mortality, revealing a nonredundant role of YB-1 in late embryonic development. Fibroblasts derived from *YB-1*$^{-/-}$ embryos displayed a normal rate of protein synthesis and minimal alterations in the transcriptome and proteome but demonstrated reduced abilities to respond to oxidative, genotoxic, and oncogene-induced stresses. *YB-1*$^{-/-}$ cells under oxidative stress expressed high levels of the G_1-specific CDK inhibitors p16Ink4a and p21Cip1 and senesced prematurely; this defect was corrected by knocking down CDK inhibitor levels with specific small interfering RNAs. These data suggest that YB-1 normally represses the transcription of CDK inhibitors, making it an important component of the cellular stress response signaling pathway.

Over the past decade, an increasing number of multifunctional regulatory factors that control gene expression at both the transcriptional and posttranscriptional levels have been described. Human YB-1 and its vertebrate homologues are one example. YB-1 belongs to a large family of proteins that contain a conserved nucleic acid-binding domain termed the *c*old *s*hock *d*omain (CSD), which shares about 40% amino acid sequence identity with bacterial cold shock proteins. Among the CSD family of proteins, YB-1 and its orthologues constitute an exceptionally conserved subfamily that contains nearly identical amino acid sequences for the whole molecule (>98% identity between the human and mouse proteins). While several members were initially identified as DNA-binding proteins that interacted specifically with a conserved *cis*-regulatory Y-box element, YB-1 proteins have since been shown to bind avidly in vitro to a wide variety of forms of nucleic acids, including pyrimidine-rich single-stranded DNA, triplex/single-stranded H-DNA, damaged DNA, and RNA (references 18 and 36 and references therein).

Based on its broad nucleic acid-binding properties, a myriad of cellular functions have been ascribed to YB-1. In mammalian cells, YB-1 has been shown to shuttle between the nuclear and cytoplasmic compartments (reference 25 and references therein). Within the nucleus, YB-1 interacts directly with other DNA- and pre-mRNA-binding proteins such as p53, AP2, CTCF, hnRNP K, and SRp30c (for a complete list, see a recent review [20]). To date, YB-1 has been implicated in nuclear activities such as chromatin remodeling, transcriptional regulation, DNA repair, and pre-mRNA splicing/transport (11). YB-1 is also abundant in the cytoplasm, where it is a major structural component of messenger ribonucleoprotein complexes and may act as an mRNA chaperone (6, 9) and a regulator of translation (reference 1 and references therein). Thus, YB-1 has been proposed to function as a multifunctional coordinator for the control of gene expression in both the nucleus and the cytoplasm (20, 34).

YB-1 is broadly expressed throughout development, and its expression level closely correlates with the cell proliferation state. *YB-1* is abundantly expressed in early chicken and rat embryos, and its level decreases steadily during development (15, 19). High levels of YB-1 are also detected in vivo in actively proliferating adult tissues such as the colorectal epithelial glands (29) and regenerating liver tissue following chemical-induced damage (15) or hepatectomy (19). *YB-1* is induced in various cell types in response to mitogenic stimuli, such as cytokine-stimulated T cells (27), serum-activated fibroblasts (19), and agonist-stimulated endothelial cells (31). Furthermore, increased nuclear and/or cytoplasmic expression of *YB-1* has frequently been detected in a wide range of human cancers, including breast, ovarian, thyroid, and colorectal cancers, osteosarcomas, and synovial sarcomas (reviewed in reference 20). Similar results have also been described for experimental systems such as mouse and rabbit cancers (reviewed in reference 21). Importantly, an association of elevated levels of YB-1 and tumor progression has been reported for melanoma and also for lung, squamous cell, and prostate cancers (21). These clinical observations have suggested that disregulated expression of *YB-1* may be associated with unfavorable clinical outcomes. However, it remains unclear whether YB-1 overex-

* Corresponding author. Mailing address: Division of Oncology, Section of Stem Cell Biology, Campus Box 8007, 660 South Euclid Ave., St. Louis, MO 63110-1093. Phone: (314) 362-8831. Fax: (314) 362-9333. E-mail: tley@im.wustl.edu.

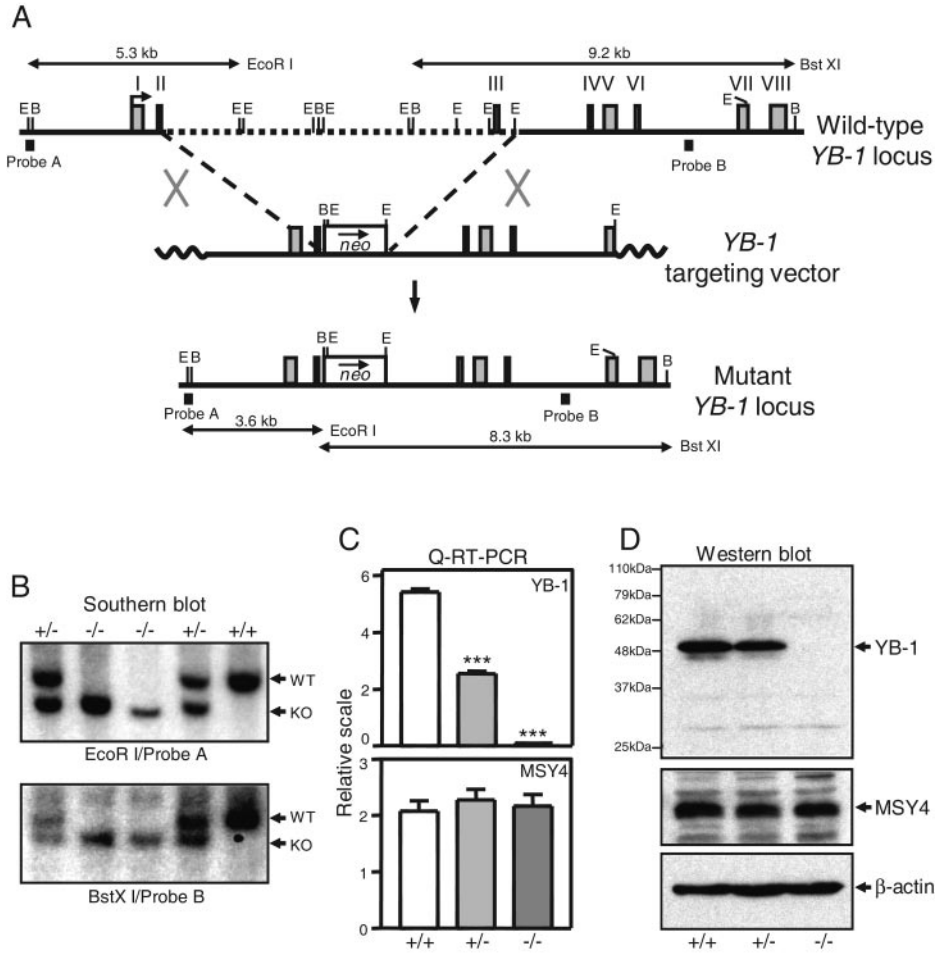

FIG. 1. Targeted disruption of *YB-1* gene. (A) Diagram of mouse *YB-1* genomic locus, targeting vector, and targeted locus. E, EcoRI; B, BstXI. (B) Southern blot analysis of genomic DNAs derived from embryos of *YB-1*$^{+/-}$ intercross. WT, wild-type allele; KO, targeted allele. (C) Real-time quantitative RT-PCR analysis of YB-1 and MSY4 mRNA expression. The data shown are mean values with standard deviations for three wild-type, three *YB-1*$^{+/-}$, or five *YB-1*$^{-/-}$ samples (***, $P < 0.001$). (D) Western blot analysis of whole-cell lysates from MEFs of each genotype with YB-1-, MSY4-, and β-actin-specific antibodies.

pression is causally related to the malignant phenotype or is simply a "marker" associated with rapid cell growth. Furthermore, the normal physiological role of YB-1 has yet to be defined, since knockout mice have been difficult to generate (28).

To better understand the physiological functions of YB-1 in vivo, we created homozygous mice with a true null mutation in the *YB-1* gene. An analysis of *YB-1*-deficient animals revealed that *YB-1* is required for the normal development of multiple embryonic organ systems and for perinatal survival. YB-1 plays an important role in cellular stress responses and in the prevention of premature senescence in cultured primary cells. YB-1 is therefore essential for early mammalian development and important for cellular responses to a variety of stresses.

MATERIALS AND METHODS

Generation of *YB-1*$^{-/-}$ mice. The left arm of the targeting vector consisted of a 3.2-kb HindIII fragment containing *YB-1* exons 1 and 2. The right arm was a 5.5-kb EcoRI fragment containing exons 4 to 6 and the 5′ portion of exon 7. The left arm, the PGK-neo cassette, and the right arm were cloned in the proper orientation into pCR2.1 (Invitrogen). The targeting vector was linearized with XhoI and electroporated into RW4 embryonic stem (ES; 129/SvJ) cells. G418-resistant clones were isolated and screened for homologous recombination by Southern analysis (Fig. 1A). A 5′ external probe (probe A) detected a 5.3-kb wild-type or 3.5-kb mutant allele in EcoRI-digested ES cell genomic DNAs. Correct targeting at the 3′ end was analyzed by Southern blotting with an internal probe (probe B). The wild-type allele generated a 9.2-kb BstXI fragment, and the mutant generated an 8.3-kb fragment. Targeted ES cell clones were injected into C57BL/6 mouse blastocysts to generate chimeras. To obtain pure 129/SvJ mice, we crossed chimeric males with 129/SvJ females to derive F1 YB-1$^{+/-}$ mice. To derive embryos of each *YB-1* genotype, we intercrossed *YB-1*$^{+/-}$ females with *YB-1*$^{+/-}$ males and designated the time for detection of a vaginal copulation plug as embryonic day 0.5 (E0.5).

MEF preparation and culture. Mouse embryonic fibroblasts (MEFs) were dissociated from E13.5 embryos with trypsin and then cultured in Dulbecco's modified Eagle's medium (Cellgro and Sigma) containing 10% heat-inactivated fetal calf serum, 1 mM sodium pyruvate, 1 mM nonessential amino acids, and 100 U/ml penicillin and streptomycin in 5% CO_2 at 37°C. For serial passaging, cells were maintained according to a protocol in which 8×10^5 cells were seeded per T-25 flask (or equivalent) every 3 days (3T8 protocol). For growth curve assays, MEFs were seeded at 3.0×10^4 cells per 12-well plate and grown for up to 12 days. MEFs were also cultured in 3% O_2–5% CO_2 in a hypoxia chamber (StemCell Technologies) at 37°C. The chamber was flushed with 3% O_2–5% CO_2 every 24 h. For synchronization of the MEFs at the G_0 phase, log-phase MEFs were washed twice with phosphate-buffered saline and incubated in Dulbecco's modified Eagle's medium supplemented with 0.1% fetal calf serum for 3 days, with the medium being changed daily. To test their sensitivity to genotoxic drugs, we seeded MEFs at 3.0×10^4 cells per 12-well plate and allowed them to attach by

incubating overnight. The cells were then exposed to various doses of drugs (see Fig. 4C) for 3 h, washed with medium, and cultured for 3 more days before being counted. Cell growth was expressed as a percentage of the growth by control MEFs of each genotype without drugs.

BrdU incorporation, ^{35}S incorporation, and senescence-associated β-galactosidase (SA-β-Gal) assay. For 5-bromo-2′-deoxyuridine (BrdU) labeling, MEFs were incubated in culture medium containing 10 μM BrdU (Roche) for 30 min at 37°C and then processed as suggested by the kit manufacturer.

For determination of the rate of protein synthesis, cells were washed twice with labeling medium (MP Biochemicals) and then incubated in the same medium containing 30 to 100 μCi/ml Trans[^{35}S] label (MP Biomedicals) for 30 min at 37°C. To inhibit protein synthesis, we allowed the labeling reaction to proceed in the presence of 50 μg/ml cycloheximide (Sigma). For determination of the amount of ^{35}S label incorporation, the samples were harvested, total cell numbers were counted, and then the samples were treated with trichloroacetic acid (TCA). The radioactivity present in the TCA precipitates was measured by liquid scintillation counting and normalized to the cell number.

The SA-β-Gal activity at pH 6.0 was assayed by flow cytometry using an ImaGene Green C_{12}FDG *lacZ* gene expression kit as described by the manufacturer (Molecular Probes), with small modifications. Briefly, harvested cells were fixed for 3 min with 3% formaldehyde at room temperature, washed with phosphate-buffered saline, stained for 1 h with the SA-β-Gal stain solution described by Dimri et al. (7), using C_{12}FDG in place of X-Gal (5-bromo-4-chloro-3-indolyl-β-D-galactopyranoside), and immediately analyzed with a FACScan cytometer.

Antibodies and Western analysis. We generated rabbit antisera against a mouse YB-1 peptide (QPREDGNEEDKEN; residues 252 to 264) and an MSY4 peptide (NRMQAGEIGEMKDGV; residues 249 to 263). Additional primary antibodies used were anti-actin (C-20; Santa Cruz), anti-p16Ink4a (M-156; Santa Cruz), anti-p21Cip1 (Ab-6; Oncogene), anti-Mdm2 (SMP-149; Santa Cruz), anti-p53 (Ab-7; Oncogene), and anti-green fluorescent protein (anti-GFP) (fl-1; Santa Cruz). Western blotting was performed according to a standard procedure (18) or as recommended by the suppliers, and proteins were detected by enhanced chemiluminescence using the ECL detection system (Amersham).

Lentivirus production and infection and small interfering RNA (siRNA) infection. A YB-1–GFP fusion cDNA was created by cloning the human YB-1 cDNA into HindIII and BamHI sites of pEGFP-N1 (Clontech) and subcloning this vector into a lentiviral transfer vector. To infect MEFs with the virus, we incubated 2×10^5 log-phase cells in media containing different virus titers, and we analyzed the efficiency of infection by determining the percentage of GFP$^+$ cells with a FACScan cytometer at 2 days postinfection.

The sense sequence of the siRNA specific for p16Ink4a was 5′-GGAGUCC GCUGCAGACAGAdAdT-3′, which is encoded by exon 1 of the gene. The sense sequence of the siRNA for a knockdown p21Cip1 mRNA was 5′-AACG GUGGAACUUUGACUUCG-3′ and was previously described (38). A nonspecific control duplex with 47% GC content and UU overhangs which lacks homology with known gene targets (Dharmacon) was used as a nontargeting siRNA control. siRNA transfection was performed as previously described (38).

Microarray and DIGE analysis. Total RNAs were isolated from passage 3 MEFs by use of an RNeasy kit (QIAGEN). Microarray probes were synthesized by using individual RNA samples and were hybridized with Affymetrix mouse MU74Av2 GeneChips at the Siteman Cancer Center Multiplexed Gene Analysis Core. The data set was analyzed with the Significance Analysis of Microarrays (SAM) program to identify transcripts that were differentially displayed among *YB-1*$^{+/+}$, *YB-1*$^{+/-}$, and *YB-1*$^{-/-}$ MEFs. Specifically, a two-class unpaired permutation test using a twofold-change threshold was used to determine significantly changed transcripts. A statistic tuning parameter (Δ value) was used to adjust the stringency of analysis (i.e., the predicted median false discovery rate [up to 0.140]). Whole-cell lysates were prepared from passage 3 MEFs for two-dimensional (2-D) differential in-gel electrophoresis (DIGE) analysis as previously described (5).

RESULTS

Targeted inactivation of *YB-1*. To study the normal functions of *YB-1* in mice, we used homologous recombination to generate a true null allele of *YB-1* in 129/SvJ mouse ES cells. The strategy used to disrupt the gene is illustrated in Fig. 1A. Homologous recombination between the targeting vector and the *YB-1* locus results in the replacement of a 9.5-kb genomic region containing *YB-1* exon 3 with a PGK-neo cassette. The deleted exon 3 encodes a portion of the YB-1 CSD, and the mutation also disrupts the coding frame of the gene. Two correctly targeted clones were identified by Southern blot analysis (see Materials and Methods); both were injected into C57BL/6 mouse blastocysts to generate chimeras. Germ line transmission of the mutation was achieved by both lines of chimeric males when they were bred with C57BL/6 female mice. The two resultant mutant strains displayed the same phenotypes, and both were used to obtain the data presented in this report.

Embryos homozygous for the *YB-1* targeted mutation were recovered from *YB-1*$^{+/-}$ intercross matings (Fig. 1B and 2A). To measure the transcriptional output from the mutant allele, we performed real-time quantitative RT-PCR analysis of total RNAs derived from cells of individual embryos. Two primer sets (one downstream and one upstream of the deleted exon 3) gave similar results (Fig. 1C and data not shown). No *YB-1* mRNA was detected in *YB-1*$^{-/-}$ cells. *YB-1*$^{+/-}$ samples showed an approximately 50% reduction in the levels of *YB-1* mRNA ($P < 0.001$). Western blot analysis using an antibody against a peptide C-terminal to the CSD revealed the complete absence of the YB-1 protein in E13.5 *YB-1*$^{-/-}$ embryos (Fig. 1D). The steady-state mRNA and protein levels of the *MSY4* gene (a *YB-1* paralogue coexpressed with *YB-1* in developing embryos) were not altered in *YB-1*$^{+/-}$ or *YB-1*$^{-/-}$ embryos (Fig. 1C and D).

Disruption of *YB-1* results in embryonic/perinatal lethality. Mice heterozygous for the *YB-1* mutation were phenotypically indistinguishable from their wild-type littermates. However, no homozygous pups were detected at weaning in a total of 482 progeny produced from 90 *YB-1*$^{+/-}$ intercrosses (Fig. 2A, 129/SvJ × C57BL/6, stage 3W). The ratio of *YB-1*$^{+/+}$ to *YB-1*$^{+/-}$ mice (164:318) was approximately 1:2. Similar results were obtained from pure 129/SvJ *YB-1*$^{+/-}$ matings (stage 3W).

Next, we sought to determine when the mortality of *YB-1*$^{-/-}$ mice occurs. *YB-1*$^{+/-}$ females used for intercross matings were sacrificed at various gestational stages, genotypes of individual embryos were determined by Southern blotting and PCR analysis, and the results are summarized in Fig. 2A. At embryonic day 13.5 (E13.5), 4 of 39 homozygous embryos were nonviable, as indicated by partial embryonic resorption or a lack of cardiac activity and reflex motion. By E15.5, the fraction of nonsurviving *YB-1*$^{-/-}$ embryos was ~27% (4/15). The majority of homozygous embryos (14/18) were still alive near the end of gestation (E18.5). In contrast, on postnatal day 1, the frequency of homozygous neonates recovered was dramatically underrepresented. Except for one newborn, none of the *YB-1*$^{-/-}$ mutants was alive at this stage. This observation supports the hypothesis that most *YB-1*$^{-/-}$ embryos that survived to term died shortly after birth and were cannibalized.

As shown in Fig. 2B to I, *YB-1*$^{-/-}$ embryos were generally smaller than their wild-type and *YB-1*$^{+/-}$ littermates. Embryonic growth retardation was detected in most living homozygotes at E13.5 and was increasingly prominent at later stages. By E18.5, the body weights of surviving homozygotes were 50 to 75% that of their wild-type and heterozygous littermates (Fig. 2J). In addition, about one-third of the *YB-1*$^{-/-}$ embryos (21/72) also displayed craniofacial lesions, including improper neural tube closure (Fig. 2C) and exencephaly (Fig. 2E, G, and I). No such abnormalities were observed with wild-type em-

A

Genotype and phenotype distribution of progeny from *YB-1*$^{+/-}$ intercross

Genetic Background	Stage	Number of litters		Genotype: alive (dead)			*YB-1*$^{-/-}$ with exencephaly††
		Line 7	Line 1 32	+/+	+/-	-/-	
129/SvJxC57Bl/6	E13.5	10	6	34	91	35 (4)	8
	E15.5	6	3	19 (1)	39	11 (4)	4
	E18.5	6	6	21	38	14 (4)	9
	P1	5	4	18	43 (1)	1†(5)	1
	3W	43	47	164	318	0	0
129/SvJ	3W	5	6	15	20	0	0

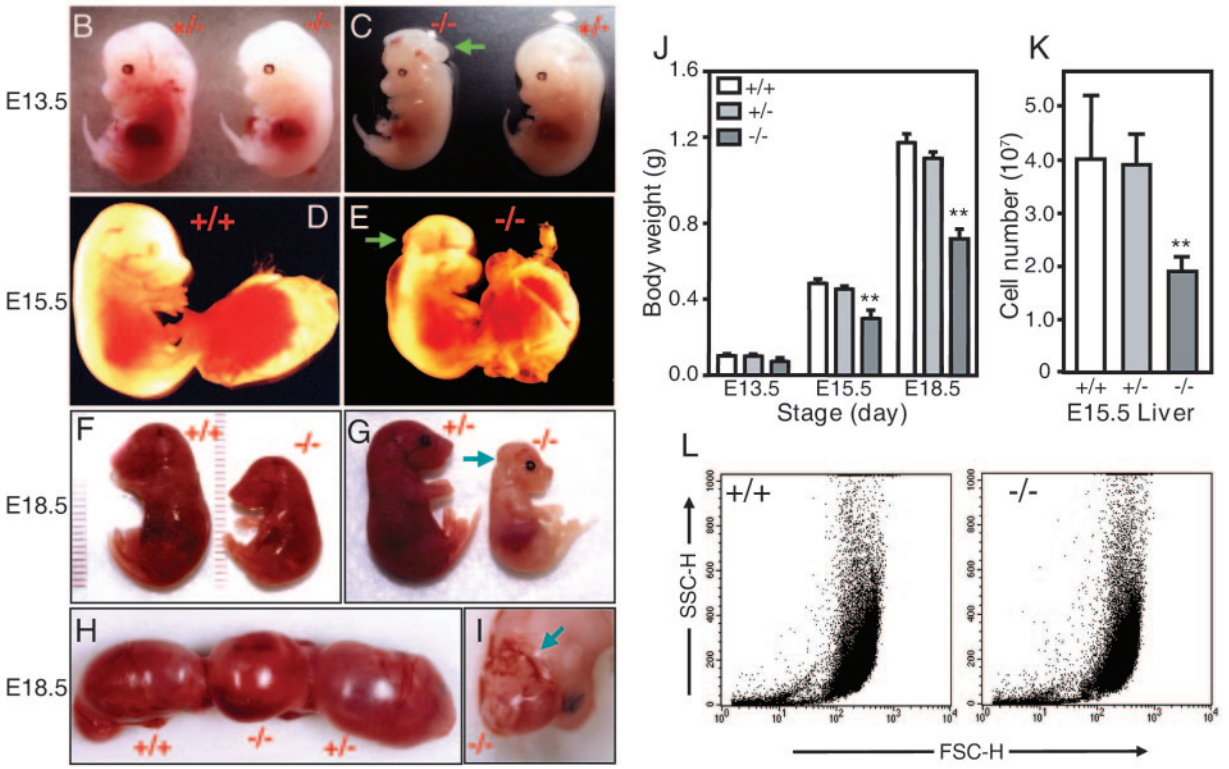

FIG. 2. Phenotypes of *YB-1*$^{-/-}$ embryos. (A) Genotypic and phenotypic distribution of progeny from *YB-1*$^{+/-}$ intercross. The numbers of embryos/neonates of each genotype at different stages of development are shown. The numbers of dead embryos/neonates are shown in parentheses. E, embryonic stage in days; P1, postnatal day 1; 3W, 3 weeks after birth. †, this pup was small for its age but was alive 2 h after surgical birth; ††, no wild-type or *YB-1*$^{+/-}$ mice exhibited exencephaly. (B to I) Embryos at E13.5 (B and C), E15.5 (D and E), and E18.5 (F to I) stages of development are shown. *YB-1*$^{-/-}$ embryos exhibiting craniofacial defects are noted with arrows. (J) Body weights of embryos of each genotype at different developmental stages. The data shown are mean values with standard deviations for 4 to 7 wild-type, 9 to 14 *YB-1*$^{+/-}$, and 3 to 10 *YB-1*$^{-/-}$ embryos (**, $P < 0.01$). (K) Mean numbers of cells in fetal livers of four wild-type, four *YB-1*$^{+/-}$, and four *YB-1*$^{-/-}$ E15.5 embryos, with standard deviations (**, $P < 0.01$). (L) Flow cytometry-based morphological analysis of liver cells from one wild-type and one *YB-1*$^{-/-}$ E15.5 embryo.

bryos or heterozygotes. All embryos with craniofacial defects were markedly pale, perhaps as a consequence of severe blood loss from cerebral hemorrhage (Fig. 2H and I). Of these, one-third (3/9) did not survive to E18.5, and the remainder died shortly after C-section. The majority of E18.5 *YB-1*$^{-/-}$ embryos without exencephaly (8/9) were initially alive but quickly became cyanotic. Five of eight such neonates lost viability within the first hour, whereas all wild-type ($n = 21$) and *YB-1*$^{+/-}$ neonates ($n = 38$) were viable at this point. Histological analyses of serial embryo sections revealed that the alveolar spaces in the lungs of dead E18.5 ($n = 2$) and P1 ($n = 1$) mutants were not inflated (data not shown). The other major organ systems of these animals were small but grossly normal. Taken together, these data suggest that neurological lesions, severe hemorrhage, and respiratory failure at least partially account for the observed embryonic/perinatal lethality.

Multiorgan hypoplasia in *YB-1*$^{-/-}$ embryos. We next examined the organs of YB-1-deficient embryos to define the number and size of their constituent cells. The number of cells recovered from E15.5 *YB-1*$^{-/-}$ livers was about 50% that of their wild-type and heterozygous counterparts ($P < 0.01$; Fig. 2K). The undergrowth defect was not due to a developmental arrest, since the onset of fetal/adult hematopoiesis occurred in E13.5 *YB-1*$^{-/-}$ livers without a noticeable delay (Z. H. Lu and T. J. Ley, unpublished data). Similarly, there were about 40% fewer cells recovered from trypsin-digested E13.5 *YB-1*$^{-/-}$ carcasses (embryos with neurological tissues and internal organs removed [data not shown]). Flow cytometric analysis revealed similar forward- versus side-scatter profiles for both fetal hepatocytes (Fig. 2L) and fibroblasts (data not shown) obtained from all embryos tested, suggesting that *YB-1* deficiency does not alter the size or granularity of these cell types in vivo. We next performed terminal deoxynucleotidyltransferase-mediated dUTP-biotin nick end labeling (TUNEL) assays on serial cryo-sections of E18.5 embryos and found that the *YB-1*$^{-/-}$ tissues contained normal numbers of TUNEL$^+$ cells relative to wild-type samples (data not shown). These data suggest that *YB-1*$^{-/-}$ embryos manifest growth retardation as a result of multiorgan hypoplasia (a defect in cellular proliferation) without detectable cellular hypotrophy (undergrowth of cell mass) or increased apoptosis.

***YB-1* deficiency does not cause "global" changes in the transcriptome, proteome, or rate of protein synthesis in cells derived from developing embryos.** Since YB-1 has been proposed to act as an important transcription/mRNA stability factor for a variety of genes that could be relevant for embryonic development, we performed a microarray analysis of cells derived from individual embryos to identify genes with altered expression patterns due to the loss of *YB-1*. Total RNAs were isolated from primary fibroblasts which had been freshly established from E13.5 wild-type ($n = 2$), *YB-1*$^{+/-}$ ($n = 4$), or *YB-1*$^{-/-}$ ($n = 4$) embryos (MEFs), labeled, and hybridized with Affymetrix mouse MU74Av2 chips. The left panel of Fig. 3A shows a scatter plot of the average signal of *YB-1*$^{-/-}$ samples for each probe set on the *y* axis, with corresponding average wild-type signals shown on the *x* axis. The microarray data set was analyzed with the SAM program to identify mRNAs that were differentially displayed from MEFs derived from *YB-1*$^{+/+}$/*YB-1*$^{+/-}$ embryos ($n = 6$) versus those from *YB-1*$^{-/-}$ embryos ($n = 4$) (Fig. 3A, right panel). Using nonstringent parameters (with a twofold-change cutoff and a relaxed false discovery rate [median = 14%; 90% percentile = 42%]), we found that YB-1 itself displayed a greatly reduced abundance (>24-fold) in *YB-1*$^{-/-}$ cells. Four mRNAs displayed a small increase in abundance (more than twofold but less than threefold) (adenylyl cyclase-associated CAP protein homolog 1, Gap junction membrane channel protein β2, translation elongation factor 1 homolog β2, and cardiac α-actin), and only one other mRNA was reduced more than twofold (FMS-like tyrosine kinase 1). These results, together with the observation that the total RNA yields per cell were indistinguishable among all samples studied, strongly suggest that the transcriptome is not globally altered in E13.5 embryonic tissues deficient in YB-1.

We next performed a proteomic analysis of fibroblasts from individual embryos to define alterations in steady-state protein levels. Two sets of *YB-1*$^{-/-}$ and wild-type MEFs which were freshly derived from two independent litters were subjected to 2-D-DIGE analysis. Figure 3B shows a representative pair of 2-D gel profiles for one set of MEFs. Murine YB-1 (pI of 9.88) was outside the range of proteins that were resolved on this gel. With a cutoff of a twofold minimal change, the statistical significance analysis failed to identify any protein spots that were consistently different between two independent paired sets.

YB-1 has been proposed to play a role in the global regulation of mRNA translation. We therefore performed a *trans*-^{35}S label incorporation assay with freshly established MEFs. The amount of protein synthesis in serum-starved or restimulated *YB-1*$^{-/-}$ MEFs was compared with that in wild-type MEFs (Fig. 3C). The protein synthesis inhibitor cycloheximide was used to verify that *trans*-^{35}S label incorporation exclusively measured protein synthesis. As shown in Fig. 3D, there was no detectable difference in ^{35}S label incorporation into proteins (on a per cell basis) between freshly prepared quiescent *YB-1*$^{-/-}$ and wild-type MEFs. In addition, *YB-1*$^{-/-}$ and wild-type MEFs showed similar increases in ^{35}S label incorporation in response to mitogen stimulation.

***YB-1*$^{-/-}$ MEFs display an elevated sensitivity to oxidative, genotoxic, and oncogene-induced stresses.** We next cultured MEFs from individual E13.5 *YB-1*$^{-/-}$ embryos to test the effect of YB-1 deficiency on cellular growth in vitro under conditions of oxidative stress (20% O_2) or under "physiological" conditions (3% O_2) (24). MEFs were cultured and serially passaged according to a 3T8 protocol, and their cell numbers were monitored at the end of each passage. As expected, wild-type (Fig. 4A) and *YB-1*$^{+/-}$ cells (data not shown) proliferated rapidly in early passages but showed a steady decline in the rate of cell growth in 20% O_2. In contrast, *YB-1*$^{-/-}$ MEFs exhibited lower cell densities throughout the early passages and entered complete growth arrest as early as passage 4, two to three passages earlier than the wild-type cells. In 3% O_2, both wild-type and *YB-1*$^{-/-}$ MEFs showed significantly prolonged proliferative life spans. As shown in Fig. 4B, a lower seeding density did not release the growth arrest of *YB-1*$^{-/-}$ cells grown in 20% O_2 (passage 5), ruling out the possibility that an increased sensitivity to contact inhibition (which is reversible) was responsible. In addition, *YB-1*$^{-/-}$ MEFs also displayed an increased sensitivity to the genotoxic drugs mitomycin C and cisplatin compared with *YB-1*$^{+/+}$ and *YB-1*$^{+/-}$ MEFs (Fig. 4C), and they had a reduced proliferative response to c-Myc overexpression (data not shown).

***YB-1*$^{-/-}$ MEFs cultured in 20% O_2 senesce prematurely.** To determine the effects of *YB-1* deficiency under conditions of oxidative stress, we subjected exponentially growing, asynchronous passage 3 MEFs serially passaged in 20% O_2 to flow cytometric analysis to define their DNA contents. The extent of apoptosis was evaluated by measuring the proportion of cells containing sub-G_0/G_1 DNA content (Fig. 4D) and also by assessing the number of nonadherent cells in the medium (data not shown). No excess of apoptotic cells was detected in either assay.

YB-1$^{-/-}$ MEFs exhibited a slightly higher percentage of cells in G_0/G_1, with a smaller proportion of cells in the S and G_2/M phases (Fig. 4D). To more precisely define the effects of *YB-1* deficiency on cell cycle progression, we synchronized MEFs by

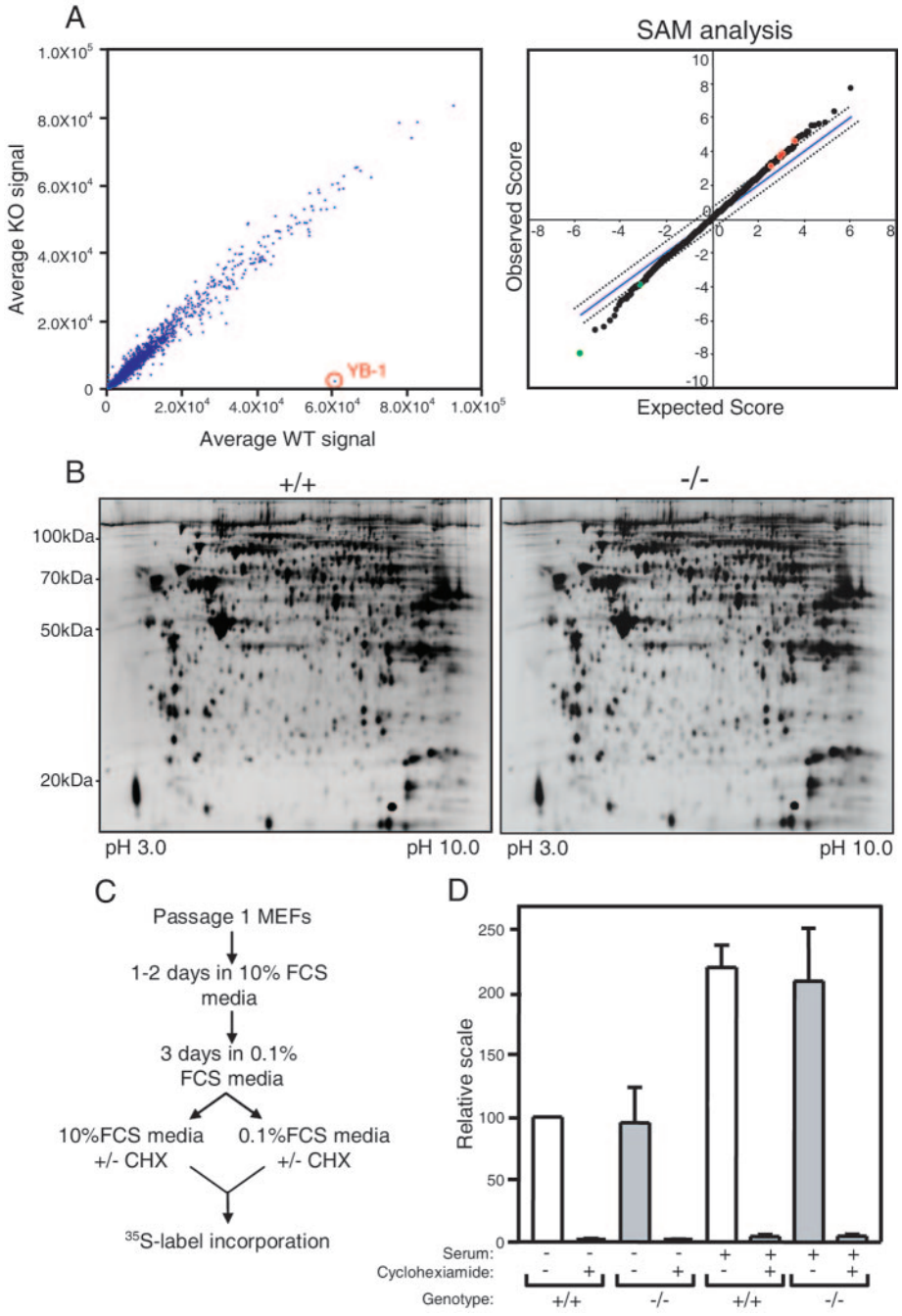

FIG. 3. *YB-1* deficiency does not cause "global" changes in transcriptome, proteome, or rate of protein synthesis in embryonic cells. (A) The left panel is a scatter plot with the average signals for each probe set of *YB-1*$^{-/-}$ samples ($n = 4$) on the *y* axis and the average wild-type signals ($n = 2$) on the *x* axis. The position of YB-1 is shown. The right panel shows a SAM analysis of the microarray data set. Spots in green and red represent genes that were significantly altered (more than twofold) in *YB-1*$^{-/-}$ samples compared to wild-type and *YB-1*$^{+/-}$ levels. (B) Proteomic analysis by 2D-DIGE of *YB-1*$^{-/-}$ and wild-type MEFs freshly established from embryos. (C) Diagram of ^{35}S labeling experiment. CHX, cycloheximide. (D) ^{35}S label incorporation assay with serum-starved or restimulated MEFs, with or without cycloheximide. Data for four wild-type and four *YB-1*$^{-/-}$ MEF samples from two independent experiments are shown, with the incorporation normalized by cell number.

serum starvation. The cells were then stimulated to reenter the cell cycle by the addition of 10% serum. Growth factor deprivation did not cause a completely irreversible growth arrest in *YB-1*-deficient cells (Fig. 4E), nor did it cause apoptosis (data not shown). We next performed a BrdU pulse-labeling assay with passage 3 MEFs to assess the timing of accumulation of S-phase cells (Fig. 4F). After a lag phase of 8 to 12 h, the wild-type cultures showed a steady increase in the proportion of S-phase cells, so that by 16 h, >55% of the cells were in S phase. In contrast, only a small proportion of *YB-1*$^{-/-}$ cells entered S phase at 12 h, and the percentage of *YB-1*$^{-/-}$ cells in S phase was consistently lower than that of wild-type cells for

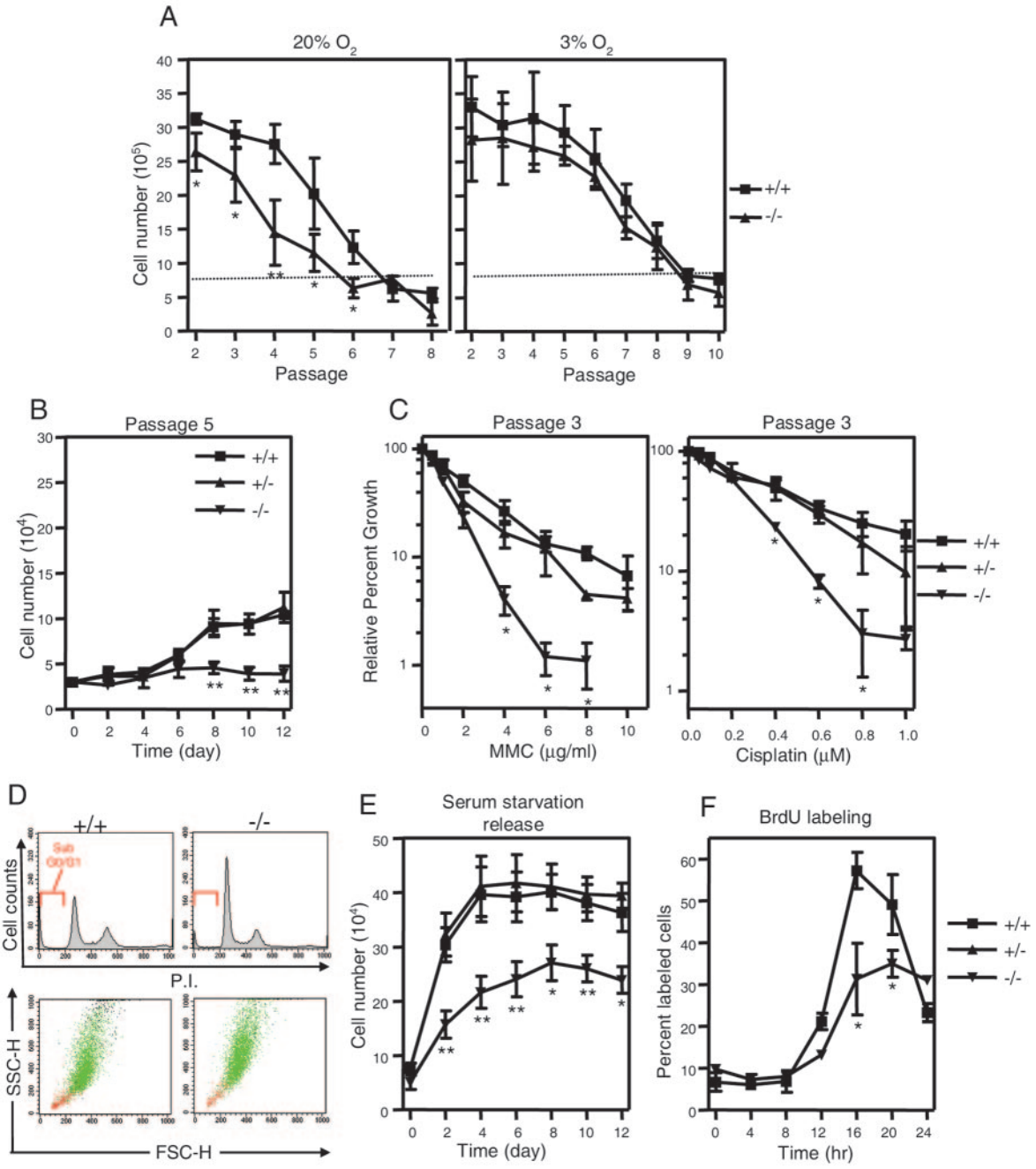

FIG. 4. *YB-1*$^{-/-}$ MEFs showed increased sensitivity to oxidative, genotoxic, and c-Myc-induced stresses. (A) Serial passaging analysis of four wild-type and four *YB-1*$^{-/-}$ MEF samples in 20% or 3% O_2. (B) Growth analysis of passage 5 MEFs serially cultured in 20% O_2. Numbers refer to mean values with standard deviations. (C) Relative growth of three wild-type, two *YB-1*$^{+/-}$, and two *YB-1*$^{-/-}$ MEF preparations exposed to various doses of mitomycin C (MMC) and cisplatin, calculated and expressed as percentages of control MEFs of each genotype without drug treatment (designated as 100%). (D) Flow cytometric analysis of cellular DNA contents (top) and flow cytometry-based analysis of cell morphology using forward- and side-scatter (FSC-H and SSC-H) parameters (bottom). The cells with sub-G_0/G_1 DNA content are marked in red. (E) Growth of serum-starved MEFs after addition of 10% serum. The numbers refer to mean values for five wild-type, five *YB-1*$^{+/-}$, and five *YB-1*$^{-/-}$ MEF preparations from two independent experiments. (F) Analysis of percentages of BrdU-labeled MEFs after the addition of serum. Mean values with standard deviations from two independent experiments are plotted. *, $P < 0.05$; **, $P < 0.01$.

up to 20 h. At this point, the majority of wild-type cells had exited S phase.

We further examined the morphology of passage 4 *YB-1*$^{-/-}$ MEFs that were serially passaged in 20% O_2 and found that most cells were large and flattened, a feature which is typical of senescent fibroblasts in culture (Fig. 5A). *YB-1*$^{-/-}$ MEFs also accumulated higher levels of endogenous senescence-associated β-galactosidase (SA-β-gal) activity (pH 6.0) than did wild-type or *YB-1*$^{+/-}$ cells ($P < 0.01$) (Fig. 5B). Collectively, these results suggest that *YB-1*$^{-/-}$ MEFs have deceased proliferative

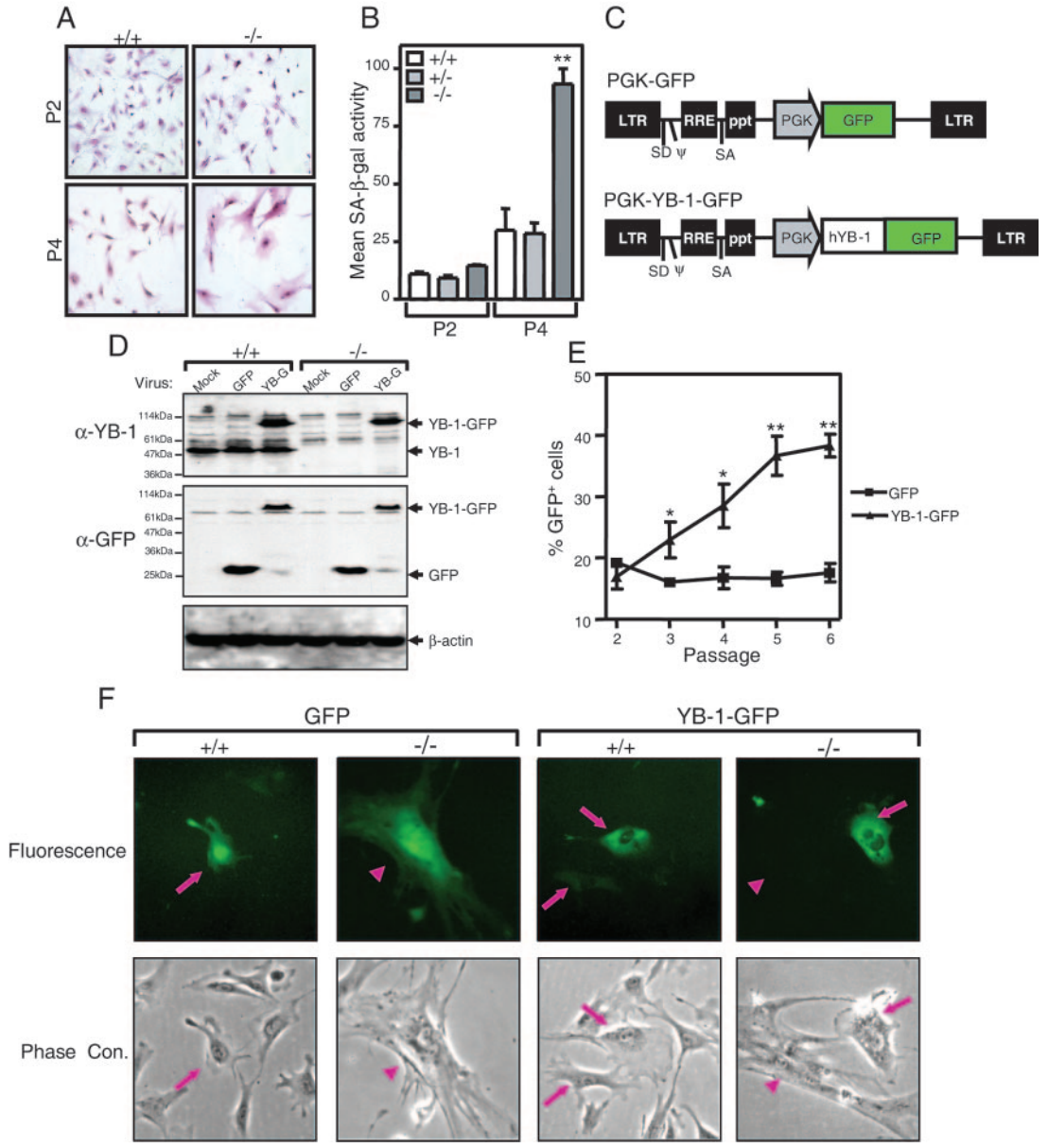

FIG. 5. Premature senescent phenotype of *YB-1*$^{-/-}$ MEFs in 20% O_2 is rescued by expression of YB-1–GFP. (A) Morphology of wild-type and *YB-1*$^{-/-}$ MEFs cultured in 20% O_2 at passages 2 and 4 after Giemsa staining. (B) Flow cytometry-based analysis of SA-β-Gal activity in MEFs. The data shown are mean fluorescence intensities of two wild-type, two *YB-1*$^{+/-}$, and two *YB-1*$^{-/-}$ MEF samples (from passages 2 and 4) from two independent experiments. **, $P < 0.01$. (C) Diagram of PGK-GFP and PGK–YB-1–GFP lentiviruses. (D) Western blot analysis of whole-cell lysates from wild-type and *YB-1*$^{-/-}$ MEFs infected with mock, GFP, or YB-1–GFP (YB-G) virus. YB-1-, GFP-, and β-actin-specific antibodies were used. (E) Serial passaging analysis of percentages of GFP$^+$ cells from *YB-1*$^{-/-}$ MEFs infected with GFP or YB-1–GFP lentivirus. The data plotted are mean values (and standard deviations) for four independent *YB-1*$^{-/-}$ MEF preparations from two independent experiments. *, $P < 0.05$; **, $P < 0.01$. (F) Fluorescence and phase-contrast microscopic analysis of wild-type and *YB-1*$^{-/-}$ passage 4 MEFs infected with GFP or YB-1–GFP lentivirus.

potential when cultured under oxidative stress because they prematurely senesce.

To determine whether the growth phenotype of YB-1-deficient MEFs is caused directly by the lack of this protein, we examined the proliferative response of *YB-1*$^{-/-}$ MEFs after the reexpression of YB-1. We used a lentivirus to introduce a PGK-driven YB-1–GFP fusion cDNA into passage 2 *YB-1*$^{-/-}$ MEFs (Fig. 5C) and then cocultured the transgene-expressing cell population with nonexpressing cells in a growth competition assay. A lentivirus that only expressed GFP was used as a negative control. The expression of YB-1–GFP was demonstrated by Western blot analysis using both YB-1- and GFP-specific antibodies (Fig. 5D). In a typical experiment, the infection of passage 2 MEFs with the YB-1–GFP- or GFP-expressing virus resulted in 13 to 21% of the cells being marked with green fluorescence (GFP$^+$) 2 days after infection (Fig. 5E). Thereafter, the cell cultures were subjected to serial passaging, and the proportion of GFP$^+$ cells was determined by

flow cytometry as a function of the passage number. The enforced expression of YB-1–GFP conferred on *YB-1*$^{-/-}$ cells a significant proliferation advantage over nonexpressing cells (Fig. 5E). The expression of GFP alone had no effect on cellular proliferation under identical conditions. The rescue of early senescence in YB-1–GFP-expressing *YB-1*$^{-/-}$ cells (but not in their GFP-expressing counterparts) was also confirmed by monitoring the total cell growth at the end of each passage (data not shown).

A microscopic analysis revealed that most passage 4 *YB-1*$^{-/-}$ cells expressing YB-1–GFP adopted a small and light-refractile morphology typical of proliferating cells (Fig. 5F, YB-1–GFP, −/−, arrows), similar to the morphology of wild-type cells (Fig. 5F, GFP, +/+, arrows). This morphology contrasted with the flattened, senescent phenotype displayed by nonexpressing cells (Fig. 5F, YB-1–GFP, −/−, arrowheads) and GFP$^+$ YB-1$^{-/-}$ cultures (Fig. 5F, GFP, −/−, arrowheads). These results, reproduced with four independent MEF preparations from individual *YB-1*$^{-/-}$ embryos, collectively suggest that the premature senescence observed in oxidatively stressed *YB-1*$^{-/-}$ MEFs is due to the *YB-1* deficiency per se and not to a "neighborhood effect" caused by the retained PGK-neo cassette.

Several regulatory pathways are altered in stressed *YB-1*$^{-/-}$ MEFs. We next examined the status of various G_1 regulatory and senescence-related proteins in *YB-1*$^{-/-}$ MEFs cultured in 20% O_2 for various periods of time. We could not detect consistent changes in the protein levels of p53, p19Arf, or CDK4 between *YB-1*$^{-/-}$ and wild-type/*YB-1*$^{+/-}$ cells as a function of the passage number (Fig. 6A and data not shown). p27Kip1 levels were high in all passage 2 MEFs but declined more rapidly in continuously passaged *YB-1*$^{-/-}$ cells than in wild-type or *YB-1*$^{+/-}$ cells. In contrast, the cyclin-dependent kinase inhibitor p16Ink4a and the p53 transcriptional targets p21Cip1 and Mdm2 accumulated more rapidly in *YB-1*$^{-/-}$ MEFs. The abundance of p16, p21, and Mdm2 in passage 3 *YB-1*$^{-/-}$ cells (lane 6) was significantly higher than that in passage 4 wild-type and *YB-1*$^{+/-}$ cells (lanes 7 and 8). The increased abundance of p16 and p21 was due to increased levels of their respective mRNAs (Fig. 6B), suggesting that a transcriptional mechanism(s) is responsible. To determine the relevance of p16 and p21 overexpression in mediating premature senescence, we "knocked down" the levels of these proteins in *YB-1*$^{-/-}$ MEFs by using specific siRNAs (Fig. 6C). As shown in Fig. 6D, the p16 and p21 double knockdown extended the proliferative capacity of late-passage *YB-1*$^{-/-}$ cells. The early senescent phenotype of *YB-1*$^{-/-}$ cells was not completely rescued by the double knockdown of p16 and p21, but not all cells were transfected and inhibition was incomplete. The double knockdown of p16 and p21 also enhanced the proliferation of wild-type cells, as predicted.

DISCUSSION

We have generated the first loss-of-function mouse model to study the physiologic roles of YB-1. We found that YB-1 plays important roles in late-stage embryonic development and is essential for survival beyond the perinatal stage. The loss of YB-1 does not cause "global" changes in the transcriptomes or proteomes of cells freshly isolated from *YB-1*$^{-/-}$ embryos. However, serially cultured *YB-1*$^{-/-}$ MEFs showed an increased sensitivity to oxidative, genotoxic, and oncogene-induced stresses in vitro. *YB-1*$^{-/-}$ MEFs cultured in 20% O_2 lost the proliferative response to serum stimulation and entered senescence prematurely; these defects were rescued by reducing the environmental O_2 to 3% or by ectopically expressing human YB-1 cDNA. We further showed that a YB-1 deficiency results in a premature accumulation of the G_1-specific cdk inhibitors p16Ink4a and p21Cip1 in cells undergoing early senescence. Knocking down the levels of these cell cycle inhibitors partially rescued the senescent phenotype of *YB-1*$^{-/-}$ cells under oxidative stress.

Our data revealed that YB-1 deficiency results in fully penetrant late embryonic runting and perinatal lethality. Morphological and histological analyses revealed that many *YB-1*$^{-/-}$ embryos displayed major developmental defects (neurological abnormalities, hemorrhage, and respiratory failure) that probably contributed to lethality. Growth retardation occurred in all late-stage embryos and was the result of hypoplasia in multiple organ systems. Since late-stage embryogenesis involves massive cellular proliferation that occurs over a very short period of time, the late embryonic period can be thought of as a time of considerable proliferative stress. The multiorgan hypoplasia observed in *YB-1*$^{-/-}$ embryos may therefore occur because of defective stress response signaling pathways in the constituent cells. This hypothesis is also consistent with the observation that YB-1 expression is elevated in many cell lines in response to various environmental stresses (see below). An alternative explanation for the late embryonic hypoplasia is a placental defect caused by YB-1 deficiency. This explanation seems unlikely to us, however; although *YB-1*$^{-/-}$ placentas were noted to be slightly smaller than those of wild-type controls, they did not display any of the abnormalities associated with placental failure (26). To formally rule out of this possibility, a conditional knockout approach with adult mice would be required.

Numerous in vitro studies have implicated YB-1 in important cellular functions such as protein synthesis, mRNA stabilization, cell cycle regulation, and cell survival. Two previous reports of targeted *YB-1* mutations in cultured cell lines (for both, only *YB-1*$^{+/-}$ cells were established) have suggested that haploinsufficient phenotypes exist. Guntaka and colleagues showed that a chicken lymphoid DT40 cell line heterozygous for a *YB-1* targeted mutation displayed major cellular defects, such as aneuploidy and severe apoptosis (33). Kuwano's group found that the disruption of one allele of the *YB-1* gene in a mouse ES cell line caused an abnormal sensitivity to external cytotoxic stimuli (28). In contrast with these studies, we showed that *YB-1*$^{+/-}$ mice and MEF preparations have no detectable phenotype. The mechanisms for the discrepancies among these mutations are currently unknown, but the two mutant alleles described in the previous studies could have potentially encoded truncated proteins that may have acted as dominant-negative molecules. Regardless, it is clear that heterozygosity for our "true null" mutation of *YB-1* supports all of the normal physiological functions of this protein in vivo.

Based on the observation of Evdokimova et al. (10) that immunodepletion of YB-1 results in a complete inhibition of protein synthesis in a rabbit reticulocyte lysate, we expected that a loss of YB-1 would not be compatible with cell viability.

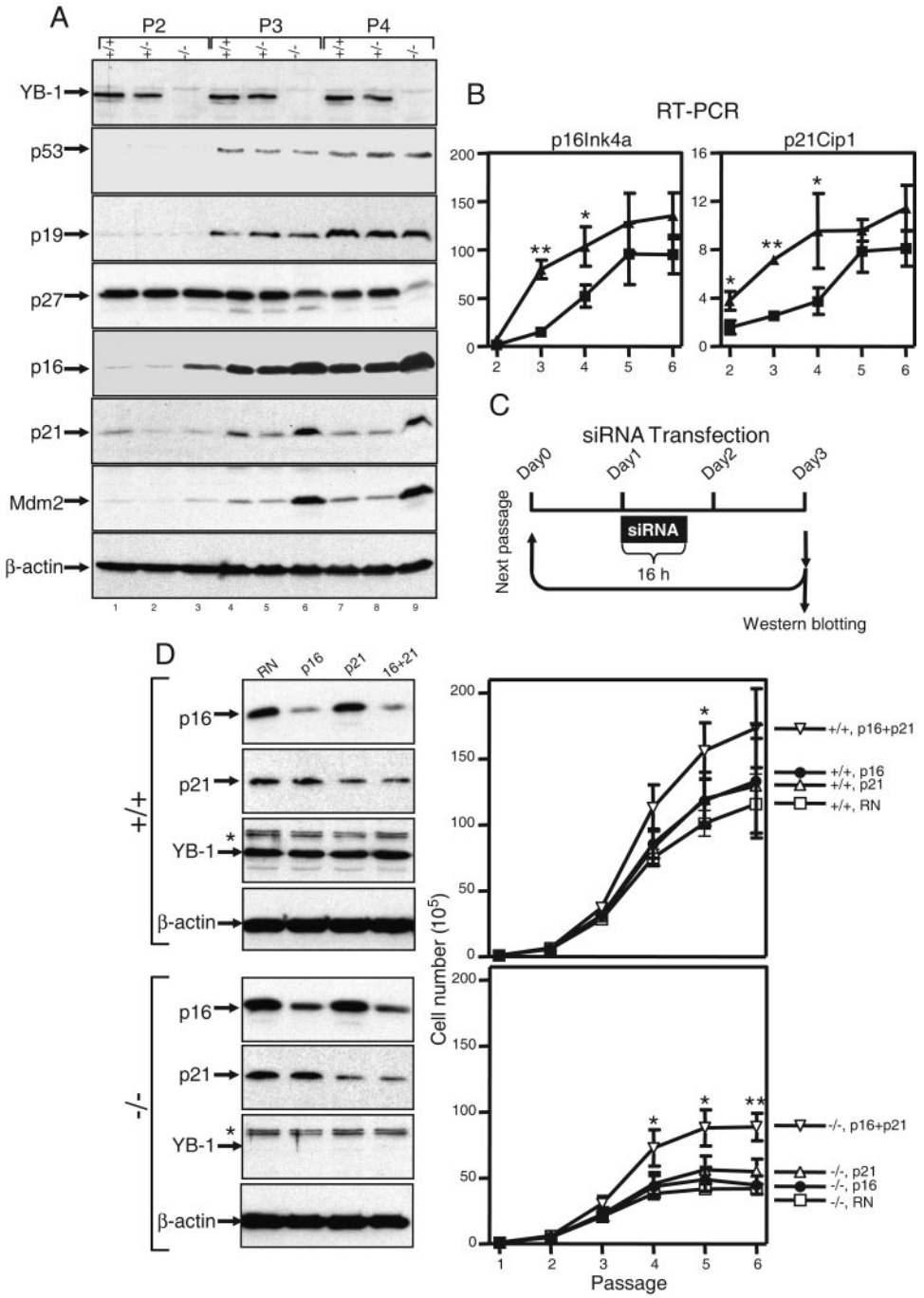

FIG. 6. Multiple cell cycle regulatory proteins are altered in *YB-1*$^{-/-}$ MEFs cultured in 20% O_2. (A) Western analysis of whole-cell lysates from MEFs of each genotype at passages 2, 3, and 4. β-Actin was used as a loading control. (B) Real-time quantitative RT-PCR analysis of p16 and p21 mRNA expression in wild-type and *YB-1*$^{-/-}$ cells. (C) Diagram of siRNA transfection protocol. (D) Western analysis of whole-cell lysates from wild-type and *YB-1*$^{-/-}$ cells 2 days after transfection with a random (RN), p16Ink4a, p21Cip1, or p16Ink4a/p21Cip1 siRNA (left). The right panels show the cumulative growth of two wild-type and four *YB-1*$^{-/-}$ MEF preparations transfected with a random (RN), p16Ink4a, p21Cip1, or p16Ink4a/p21Cip siRNA. *, nonspecific band used to predict the position of YB-1.

However, our studies with *YB-1*-deficient mice revealed that a high percentage of mouse embryos develop and survive to the late stage of embryogenesis. Furthermore, we detected "wild-type" numbers of apoptotic cells in YB-1-deficient embryos and cultured MEFs. These results strongly suggest that YB-1 is not a cell viability factor or a bona fide cell cycle regulator. We further showed that the loss of YB-1 does not cause "global" changes in the transcriptome, the proteome, or the rate of total protein synthesis in freshly isolated MEFs. These findings, while surprising, raise the possibility that other Y-box proteins may substitute for YB-1 to "rescue" these activities. Three Y-box proteins, YB-1, MSY2, and MSY4 (13, 35), have been

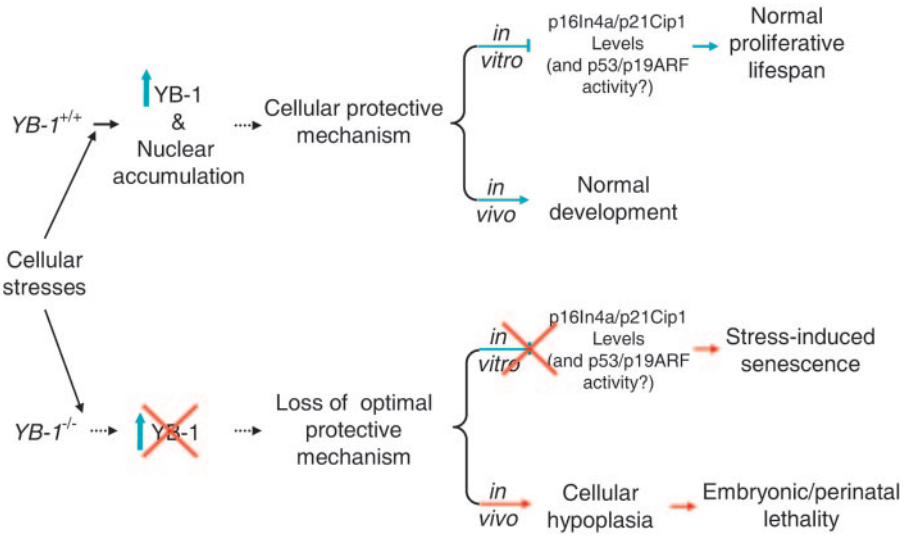

FIG. 7. Model of YB-1 function. Many environmental insults or cellular proliferation signals induce the expression and nuclear accumulation of YB-1 in mammalian cells. YB-1 is an integral part of a general cellular stress response signaling pathway required for protecting cells from a variety of stresses. The loss of YB-1 causes the loss of this protective mechanism. Consequently, cells deficient in YB-1 show an increased sensitivity to environmental stresses, leading to premature senescence.

identified in mice, and their orthologues are known from *Xenopus* to humans (4, 14). In mice, YB-1 and MSY4 are ubiquitously expressed throughout development. In addition to the highly conserved central CSD, all vertebrate Y-box proteins contain a short and variable amino-terminal domain and a long structurally conserved carboxyl tail consisting of four basic/aromatic islands. Y-box paralogues have been shown to possess similar biochemical properties in vitro (reference 13 and references therein). Regardless of these observations, YB-1 is required for normal late embryonic development and viability and for normal responses to cellular stresses; it clearly has nonredundant functions that are not compensated for by MSY4. YB-1 is distinct from other CSD family members because its exceptionally high degree of phylogenetic conservation occurs not only in the CSD but also in the rest of the molecule. Alternatively, YB-1 and MSY4 may perform similar functions in vivo but differ mainly in their tissue distribution patterns. For example, YB-1 mRNA levels are very high in human fetal brains, where *MSY4* is minimally expressed (32). The observation that neurological development is sometimes adversely affected by YB-1 deficiency (i.e., partially penetrant neural tube defects and exencephaly) therefore suggests that YB-1 may have important functions in central nervous system development. In order to better understand the functional similarities and differences among Y-box paralogues in vivo, it will be important to compare loss-of-function models of *MSY2* and *MSY4* with that of *YB-1*.

Primary MEFs proliferate only for a finite duration in vitro before irreversibly entering into a nonproliferative state called culture shock, stasis, or stress-induced senescence. Campisi and colleagues recently showed that MEFs senesce as a result of the oxidative stress imposed by culturing in 20% O_2, which is a condition used for standard tissue culture protocols (24). In addition, a variety of cytotoxic stimuli, including UV and ionizing irradiation, anticancer drug treatments, and oncogenic viral infections, have also been shown to trigger senescence both in vitro and in vivo (3). These findings have suggested that stress-related senescence may represent one of the tumor-suppressive mechanisms of somatic cells (24). Interestingly, many of the same cytotoxic stimuli that trigger senescence are also known to induce the overexpression and/or nuclear accumulation of YB-1 (2, 8, 17, 25, 30). In the present study, we found that *YB-1*$^{-/-}$ MEFs cultured in 20% O_2 prematurely senesce and have a reduced proliferative response to serum stimulation. In addition, *YB-1*$^{-/-}$ MEFs are abnormally sensitive to genotoxic drugs (mitomycin C and cisplatin) and display a reduced ability to support the accelerated proliferation caused by oncogene overexpression. Our data therefore provide an important line of genetic evidence showing that YB-1 is an important component of a cellular stress response signaling pathway that is required to protect cells from a variety of stresses.

We do not yet know how YB-1 protects cells from senescence. However, late-passage *YB-1*$^{-/-}$ MEFs displayed a high percentage of cells in G_0/G_1 and prematurely accumulated the negative cell cycle regulators p16Ink4a and p21Cip1. These findings are consistent with the view that cell cycle arrest is an important step towards the initiation of the senescent phenotype (3). As a transcription factor, YB-1 has been described to regulate (both positively and negatively) a host of target genes involved in the stress response pathway and in cell growth (references 2, 28, and 29 and references therein). However, it remains to be established whether YB-1 plays a direct role in negatively regulating p16Ink4a and p21Cip1 transcription in oxidatively stressed MEFs. In addition, YB-1 could also directly interact with other important cytotoxic stress-related factors and modulate their biological activities. YB-1 has previously been shown to physically interact with p53 both in vitro and in vivo (23, 37). The p53/Mdm2/p19Arf pathway plays an integral role in the cellular stress response, genomic integrity surveillance, and senescence pathways. While our results do not suggest that the early senescent phenotype is caused by

disregulation of *p53* or *p19ARF* gene expression, YB-1 may still play a role in this pathway by altering p53 or p19Arf activities. Indeed, two p53 transcriptional target genes (*p21Cip1* and *Mdm2*) are prematurely induced in *YB-1*$^{-/-}$ MEFs, suggesting that p53 activity does indeed increase with a YB-1 deficiency.

Alternatively, YB-1 has been shown to exhibit high affinities for damaged DNA (apurinic or cisplatin- or UV-modified DNA) and H-DNA structures, and it physically interacts with several DNA repair factors in genotoxically stressed cells (references 12 and 22 and references therein), raising the possibility that YB-1 may function directly in DNA damage recognition and/or processing. The loss of murine Fus/TLS, a YB-1-interacting multifunctional ribonucleoprotein, has been shown to cause chromosomal instability and perinatal death (16). Many mouse mutants lacking genes important for DNA repair pathways (e.g., *Xrcc2*, *Lig4*, *Xrcc4*, *Ku70*/*80*, *Pol*β, and *Xpa*) also result in a premature senescence phenotype (references 3 and 24 and references therein). Recent clinical studies have also reported a strong correlation between the nuclear level of YB-1 and the cellular resistance to chemotherapy of various primary human cancers (reviewed in reference 12). We are therefore using our YB-1-deficient mice to investigate the importance of YB-1 for DNA repair, genome stability, and the genetic interaction with the p53 pathway (Fig. 7).

In conclusion, our data have revealed that *YB-1* is required for the normal late embryonic development and survival of mice, and they suggest that YB-1 is a cellular stress response factor that is important for preventing the early onset of senescence in cultured cells in vitro. These data raise the possibility that the overexpression of *YB-1* may contribute to transformation by protecting cells that are rapidly proliferating.

ACKNOWLEDGMENTS

This work was supported by National Institutes of Health grants DK38682 (T.J.L.) and F32 HL077048 (Z.H.L.) and by a fellowship grant from Cooley's Anemia Foundation (Z.H.L.).

We thank Kelly Schrimpf and Mieke Hoock for expert blastocyst injections and animal husbandry. Philip Horwitz was responsible for the production of the polyclonal antisera against YB-1. We thank Charles Sherr, Martine Roussel, and Jason Weber for helpful discussions. The Embryonic Stem Cell Core, Multiplexed Gene Analysis Core, and Proteomics Core of Siteman Cancer Center all contributed to the execution of these studies. Nancy Reidelberger provided expert editorial assistance.

REFERENCES

1. **Bader, A. G., K. A. Felts, N. Jiang, H. W. Chang, and P. K. Vogt.** 2003. Y box-binding protein 1 induces resistance to oncogenic transformation by the phosphatidylinositol 3-kinase pathway. Proc. Natl. Acad. Sci. USA **100:** 12384–12389.
2. **Bargou, R. C., K. Jurchott, C. Wagener, S. Bergmann, S. Metzner, K. Bommert, M. Y. Mapara, K. J. Winzer, M. Dietel, B. Dorken, and H. D. Royer.** 1997. Nuclear localization and increased levels of transcription factor YB-1 in primary human breast cancers are associated with intrinsic *MDR1* gene expression. Nat. Med. **3:**447–450.
3. **Ben-Porath, I., and R. A. Weinberg.** 2004. When cells get stressed: an integrative view of cellular senescence. J. Clin. Investig. **113:**8–13.
4. **Bouvet, P., and A. P. Wolffe.** 1994. A role for transcription and FRGY2 in masking maternal mRNA within *Xenopus* oocytes. Cell **77:**931–941.
5. **Bredemeyer, A. J., R. M. Lewis, J. P. Malone, A. E. Davis, J. Gross, R. R. Townsend, and T. J. Ley.** 2004. A proteomic approach for the discovery of protease substrates. Proc. Natl. Acad. Sci. USA **101:**11785–11790.
6. **Chen, C. Y., R. Gherzi, J. S. Andersen, G. Gaietta, K. Jurchott, H. D. Royer, M. Mann, and M. Karin.** 2000. Nucleolin and YB-1 are required for JNK-mediated interleukin-2 mRNA stabilization during T-cell activation. Genes Dev. **14:**1236–1248.
7. **Dimri, G. P., X. Lee, G. Basile, M. Acosta, G. Scott, C. Roskelley, E. E. Medrano, M. Linskens, I. Rubelj, O. Pereira-Smith, M. Peacocke, and J. Campisi.** 1995. A biomarker that identifies senescent human cells in culture and in aging skin *in vivo*. Proc. Natl. Acad. Sci. USA **92:**9363–9367.
8. **Duh, J. L., H. Zhu, H. G. Shertzer, D. W. Nebert, and A. Puga.** 1995. The Y-box motif mediates redox-dependent transcriptional activation in mouse cells. J. Biol. Chem. **270:**30499–30507.
9. **Evdokimova, V., P. Ruzanov, H. Imataka, B. Raught, Y. Svitkin, L. P. Ovchinnikov, and N. Sonenberg.** 2001. The major mRNA-associated protein YB-1 is a potent 5′ cap-dependent mRNA stabilizer. EMBO J. **20:**5491–5502.
10. **Evdokimova, V. M., E. A. Kovrigina, D. V. Nashchekin, E. K. Davydova, J. W. B. Hershey, and L. P. Ovchinnikov.** 1998. The major core protein of messenger ribonucleoprotein particles (p50) promotes initiation of protein biosynthesis *in vitro*. J. Biol. Chem. **273:**3574–3581.
11. **Faustino, N. A., and T. A. Cooper.** 2003. Pre-mRNA splicing and human disease. Genes Dev. **17:**419–437.
12. **Gaudreault, I., D. Guay, and M. Lebel.** 2004. YB-1 promotes strand separation *in vitro* of duplex DNA containing either mispaired bases or cisplatin modifications, exhibits endonucleolytic activities and binds several DNA repair proteins. Nucleic Acids Res. **32:**316–327.
13. **Giorgini, F., H. G. Davies, and R. E. Braun.** 2002. Translational repression by MSY4 inhibits spermatid differentiation in mice. Development **129:**3669–3679.
14. **Gonda, K., J. Fowler, N. Katoku-Kikyo, J. Haroldson, J. Wudel, and N. Kikyo.** 2003. Reversible disassembly of somatic nucleoli by the germ cell proteins FRGY2a and FRGY2b. Nat. Cell Biol. **5:**205–210.
15. **Grant, C. E., and R. G. Deeley.** 1993. Cloning and characterization of chicken YB-1: regulation of expression in the liver. Mol. Cell. Biol. **13:**4186–4196.
16. **Hicks, G. G., N. Singh, A. Nashabi, S. Mai, G. Bozek, S. Klewes, D. Arapovic, E. K. White, M. J. Koury, E. M. Oltz, V. L. Kaer, and H. E. Ruley.** 2000. *Fus* deficiency in mice results in defective B-lymphocyte development and activation, high levels of chromosomal instability and perinatal death. Nat. Genet. **24:**175–179.
17. **Holm, P. S., H. Lage, S. Bergmann, K. Jurchott, G. Glockzin, A. Bernshausen, K. Mantwill, A. Ladhoff, A. Wichert, J. S. Mymryk, T. Ritter, M. Dietel, B. Gansbacher, and H. D. Royer.** 2004. Multidrug-resistant cancer cells facilitate E1-independent adenoviral replication: impact for cancer gene therapy. Cancer Res. **64:**322–328.
18. **Horwitz, E. M., K. A. Maloney, and T. J. Ley.** 1994. A human protein containing a "cold shock" domain binds specifically to H-DNA upstream from the human γ-globin genes. J. Biol. Chem. **269:**14130–14139.
19. **Ito, K., K. Tsutsumi, T. Kuzumaki, P. F. Gomez, K. Otsu, and K. Ishikawa.** 1994. A novel growth-inducible gene that encodes a protein with a conserved cold-shock domain. Nucleic Acids Res. **22:**2036–2041.
20. **Kohno, K., H. Izumi, T. Uchiumi, M. Ashizuka, and M. Kuwano.** 2003. The pleiotropic functions of the Y-box-binding protein, YB-1. Bioessays **25:**691–698.
21. **Kuwano, M., Y. Oda, H. Izumi, S. J. Yang, T. Uchiumi, Y. Iwamoto, M. Toi, T. Fujii, H. Yamana, H. Kinoshita, T. Kamura, M. Tsuneyoshi, K. Yasumoto, and K. Kohno.** 2004. The role of nuclear Y-box binding protein 1 as a global marker in drug resistance. Mol. Cancer Ther. **3:**1485–1492.
22. **Lenz, J., S. A. Okenquist, J. E. LoSardo, K. K. Hamilton, and P. W. Doetsch.** 1990. Identification of a mammalian nuclear factor and human cDNA-encoded proteins that recognize DNA containing apurinic sites. Proc. Natl. Acad. Sci. USA **87:**3396–3400.
23. **Okamoto, T., H. Izumi, T. Imamura, H. Takano, T. Ise, T. Uchiumi, M. Kuwano, and K. Kohno.** 2000. Direct interaction of p53 with the Y-box binding protein, YB-1: a mechanism for regulation of human gene expression. Oncogene **19:**6194–6202.
24. **Parrinello, S., E. Samper, A. Krtolica, J. Goldstein, S. Melov, and J. Campisi.** 2003. Oxygen sensitivity severely limits the replicative lifespan of murine fibroblasts. Nat. Cell Biol. **5:**741–747.
25. **Raffetseder, U., B. Frye, T. Rauen, K. Jurchott, H. D. Royer, P. L. Jansen, and P. R. Mertens.** 2003. Splicing factor SRp30c interaction with Y-box protein-1 confers nuclear YB-1 shuttling and alternative splice site selection. J. Biol. Chem. **278:**18241–18248.
26. **Roberts, A. W., L. Robb, S. Rakar, L. Hartley, L. Cluse, N. A. Nicola, D. Metcalf, D. J. Hilton, and W. S. Alexander.** 2001. Placental defects and embryonic lethality in mice lacking suppressor of cytokine signaling 3. Proc. Natl. Acad. Sci. USA **98:**9324–9329.
27. **Sabath, D. E., P. L. Podolins, P. G. Comber, and M. B. Prystowsky.** 1990. cDNA cloning and characterization of interleukin 2-induced genes in cloned T helper lymphocytes. J. Biol. Chem. **265:**12671–12678.
28. **Shibahara, K., T. Uchiumi, T. Fukuda, S. Kura, Y. Tominaga, Y. Maehara, K. Kohno, Y. Nakabeppu, T. Tsuzuki, and M. Kuwano.** 2004. Targeted disruption of one allele of the Y-box binding protein-1 (YB-1) gene in mouse embryonic stem cells and increased sensitivity to cisplatin and mitomycin C. Cancer Sci. **95:**348–353.
29. **Shibao, K., H. Takano, Y. Nakayama, K. Okazaki, N. Nagata, H. Izumi, T. Uchiumi, M. Kuwano, K. Kohno, and H. Itoh.** 1999. Enhanced coexpression of YB-1 and DNA topoisomerase II α genes in human colorectal carcinomas. Int. J. Cancer **83:**732–737.

30. **Stein, U., K. Jurchott, W. Walther, S. Bergmann, P. M. Schlag, and H. D. Royer.** 2001. Hyperthermia-induced nuclear translocation of transcription factor YB-1 leads to enhanced expression of multidrug resistance-related ABC transporters. J. Biol. Chem. **276:**28562–28569.
31. **Stenina, O. I., E. J. Poptic, and P. E. DiCorleto.** 2000. Thrombin activates a Y box-binding protein (DNA-binding protein B) in endothelial cells. J. Clin. Investig. **106:**579–587.
32. **Su, A. I., T. Wiltshire, S. Batalov, H. Lapp, K. A. Ching, J. Zhang, R. Soden, M. Hayakawa, G. Kreiman, M. P. Cooke, and J. B. Hogenesch.** 2004. A gene atlas of the mouse and human protein-encoding transcriptomes. Proc. Natl. Acad. Sci. USA **101:**6062–6067.
33. **Swamynathan, S. K., B. R. Varma, K. T. Weber, and R. V. Guntaka.** 2002. Targeted disruption of one allele of the Y-box protein gene, Chk-YB-1b, in DT40 cells results in major defects in cell cycle. Biochem. Biophys. Res. Commun. **296:**451–457.
34. **Wilkinson, M. F., and A. B. Shyu.** 2001. Multifunctional regulatory proteins that control gene expression in both the nucleus and the cytoplasm. Bioessays **23:**775–787.
35. **Yu, J., M. Deng, S. Medvedev, J. Yang, N. B. Hecht, and R. M. Schultz.** 2004. Transgenic RNAi-mediated reduction of MSY2 in mouse oocytes results in reduced fertility. Dev. Biol. **268:**195–206.
36. **Zasedateleva, O. A., A. S. Krylov, D. V. Prokopenko, M. A. Skabkin, L. P. Ovchinnikov, A. Kolchinsky, and A. D. Mirzabekov.** 2002. Specificity of mammalian Y-box binding protein p50 in interaction with ss and ds DNA analyzed with generic oligonucleotide microchip. J. Mol. Biol. **324:**73–87.
37. **Zhang, Y. F., C. Homer, S. J. Edwards, L. Hananeia, A. Lasham, J. Royds, P. Sheard, and A. W. Braithwaite.** 2003. Nuclear localization of Y-box factor YB1 requires wild-type p53. Oncogene **22:**2782–2794.
38. **Zou, X., D. Ray, A. Aziyu, K. Christov, A. D. Boiko, A. V. Gudkov, and H. Kiyokawa.** 2002. Cdk4 disruption renders primary mouse cells resistant to oncogenic transformation, leading to Arf/p53-independent senescence. Genes Dev. **16:**2923–2934.